

Triple-differential cross sections of the (π^+, pp) reaction on lithium isotopes

R. Rieder, P. D. Barnes, B. Bassalleck,* R. A. Eisenstein,[†] G. Franklin, R. Grace, C. Maher, P. Pile,[‡] J. Szymanski, and W. R. Wharton[§]
Carnegie-Mellon University, Pittsburgh, Pennsylvania 15213

F. Takeuchi
Kyoto-Sangyo University, Kyoto 603, Japan

J. F. Amann
Los Alamos National Laboratory, Los Alamos, New Mexico 87545

S. A. Dytman**
Massachusetts Institute of Technology, Cambridge, Massachusetts 02139

K. G. R. Doss^{††}
University of Washington, Seattle, Washington 98195
 (Received 21 June 1985)

The (π^+, pp) reactions on ${}^6\text{Li}$ and ${}^7\text{Li}$ have been studied at $T_\pi = 59.4$ MeV with high resolution. The first triple-differential cross sections for these reactions are presented. The data are fitted to a T matrix and compared to the $\pi^+d \rightarrow pp$ reaction. A model in which the pion is absorbed on a 3S_1 (pn) pair in the lithium nucleus describes many features of the data very well. An extrapolation of our data into unmeasured regions of phase space suggests that about 60% of the pion absorption cross section on ${}^6\text{Li}$ at 59.4 MeV goes into the (π^+, pp) channel. One surprising feature of the data is that the ${}^6\text{Li}(\pi^+, pp){}^4\text{He}(2^-)$ transition at 22.1 MeV excitation is strongly populated, similar to what is observed in the ${}^6\text{Li}(d, \alpha){}^4\text{He}$ reaction. This transition involves removing one nucleon from the $1p$ shell and one from the $1s$ shell.

I. INTRODUCTION

Pion absorption in nuclei must involve at least two nucleons to conserve energy and momentum, thus the $\pi^+d \rightarrow pp$ reaction is the most elementary pion absorption process. In heavy nuclei the pion absorption mechanism is expected to be more complicated, often involving more than two nucleons. To help understand the reaction mechanism more completely, a "transition" nucleus, where changes from the elementary $\pi^+d \rightarrow p + p$ process to where more complicated absorption processes start to manifest themselves, was studied. The lithium isotopes have simple, well-understood nuclear structure in which the $1p$ -shell nucleons are clustered into a quasideuteron or quasitriton and are loosely bound to a $(1s)^4$ alphaslike core. The states in the residual helium isotopes are delineated into well-defined excitation regions according to the removal of $(1p)^2$, $(1p1s)$, or $(1s)^2$ nucleons from the lithium target. A wide assortment of data on pion absorption in lithium nuclei has been accumulated. This includes previous (π^+, pp) studies,¹⁻³ (π^-, nn) studies,^{4,5} and inclusive (π^+, p) studies.⁶ This paper presents the first triple-differential cross sections from the ${}^6,7\text{Li}(\pi^+, 2p){}^4,5\text{He}$ reaction at $T_\pi = 59.4$ MeV. Features of the $(\pi^+, 2p)$ data are then compared with existing data in an attempt to understand better how the absorption cross section is split between the various channels and to examine other specific features of the (π^+, pp) channels.

II. EXPERIMENTAL OVERVIEW

The experimental setup in the low-energy pion (LEP) channel at LAMPF is shown in Fig. 1. Two charged particles in coincidence were detected using two solid-state spectrometers^{7,8} constructed from stacks of eight and two high purity germanium crystals, respectively. The spectrometer with only two Ge crystals had, in addition, two

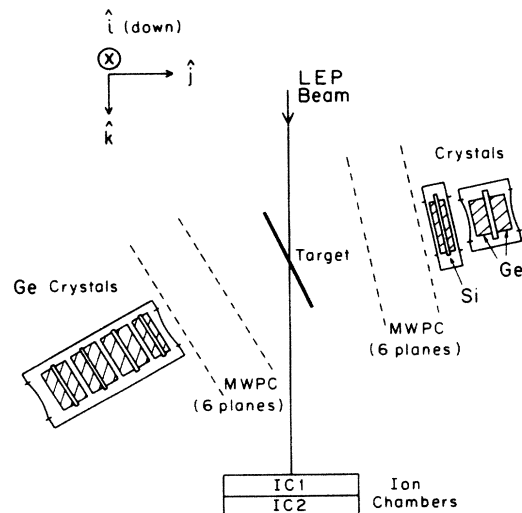


FIG. 1. A schematic diagram of the apparatus used in the experiment.

0.45 cm thick Si(Li) crystals. In front of each spectrometer were two individual wire-readout proportional chambers. Each chamber had an anode plane in the vertical, horizontal, and 45° diagonal directions (with 1 mm wire spacing), enabling the analysis of events with more than one hit in each plane. Two ionization chambers downstream of the target monitored the intensity of the incident pion beam. A three-scintillator telescope placed at a backward angle detected particles scattered from the target and provided an additional beam monitor.

The targets had thicknesses of either 100 or 150 mg/cm² of ⁶Li enriched to 95.6% and 150 mg/cm² of ⁷Li enriched to 99.9%. These targets were placed in a plastic bag 3 mil thick to minimize oxidation. The target normal was usually 65° relative to the pion beam direction. This geometry was chosen so that the direction of the two spectrometers were always within 35° of the target normal, thereby minimizing the target thickness traversed by the detected particles.

Because of the steep target angle and the large horizontal dimension of the beam, a spot approximately 10 cm wide was illuminated on the target by the beam. The vertical spot size was about 1.8 cm. The front faces of the two spectrometers were usually 20 to 25 cm from the target with Ge-crystal radii of 1.7 and 1.6 cm for the eight- and two-Ge-crystal spectrometers, respectively, resulting in effective solid angles of about 11 msr. With this geometry, each detector scanned a horizontal angular range of about ±12° and a vertical angular range of about ±4.5°.

The eight-Ge-crystal spectrometer was thick enough to stop all protons from the reactions of interest. The two-Ge-crystal spectrometer with two Si(Li) crystals in front, could stop protons with kinetic energy less than 119 MeV. Protons were identified using standard dE/dx vs E information obtained when the particle traverses at least one

crystal and stops in another crystal. This gives a low energy threshold of 26.5 and 24 MeV for identified protons in the eight-crystal and four-crystal spectrometers, respectively. Figure 2 shows a typical particle identification spectrum with a good separation of protons from deuterons and tritons.

The energy signals from each crystal were transmitted to a PDP-11/45 computer through CAMAC LRS 2259A 2048-channel analog-to-digital converters (ADC's). Both the energy calibration and the linearity were studied by setting the amplifier gains so that γ -ray sources of ⁵⁶Co, ⁶⁰Co, and ²²⁸Th covered most of the 2048-channel range of the ADC. The amplifier gains were reduced during the actual experiment to detect the charged particles. The change in amplifier gains between the γ -ray setting and the experimental setting was determined using a high-precision pulser at both gain settings. These calibrations were repeated throughout the experiment.

A fast timing signal from the first crystal of each spectrometer was used as the start and stop, respectively, of a time-to-digital converter (TDC) and provided a coincidence time resolution for (π^+ ,pp) events of ~2 ns (FWHM). Based on count rate estimates, about one percent of the events in the 5 ns wide timing peak were accidentals.

The LEP channel at LAMPF was usually run with a full-width at half maximum momentum resolution of 1 percent. During a period of low-intensity beam, wire chambers placed in the beam established the horizontal and vertical angular divergence of the beam as 6.3° and 4.3°, respectively (full width). During the experiment, chambers were not used in the beam to label the incident momentum, hence only the average pion momentum was monitored. Thus, the beam divergence contributed to the errors in the missing-momentum and missing-mass distributions. These uncertainties were incorporated into a Monte Carlo simulation of the experiment.

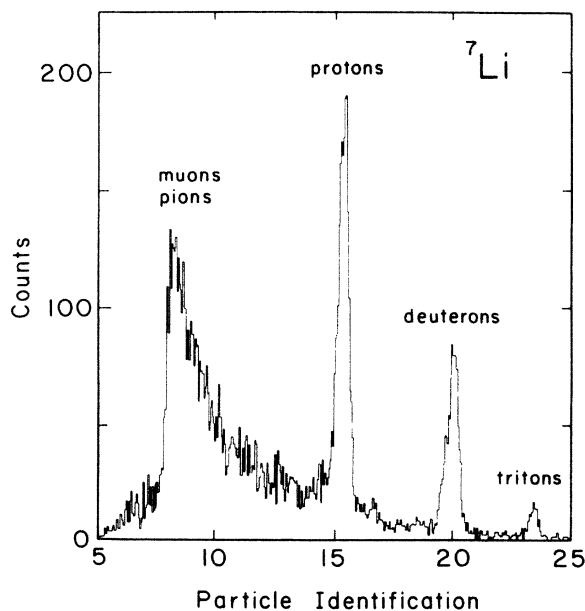


FIG. 2. A particle identification spectrum from a ⁷Li target at 80.5°. These events stopped in the second silicon detector of the four-crystal spectrometer and are in coincidence with an event in the eight-crystal spectrometer.

III. $\pi^+d \rightarrow pp$ MEASUREMENT

At various times in the experiment, data were collected on the $\pi^+d \rightarrow pp$ process using a 194 mg/cm² CD₂ target. The two-body final state was then kinematically over determined by the detection system and thus allowed its calibration. The energy calibration of each stack of detectors was found to have an error of approximately 100 keV for protons of 100 MeV. The opening angle between the two detectors had an error of 0.15° resulting from misalignment of the wire chambers. The measured angular resolution of the chambers in front of the eight-crystal spectrometer was 0.5° and 0.65° in the horizontal and vertical directions, while 1.0° and 1.2°, respectively, was obtained for the four-crystal spectrometer. These resolutions were folded quadratically with the calculated Moliere scattering in the target to estimate the overall angular uncertainty. The deuterium measurement also supplied a check on such effects as energy straggling and Moliere scattering which were included in the Monte Carlo simulation of the experiment.

A coordinate system suitable for monitoring the alignment and calibration errors is given in Fig. 3. The \hat{x} coord-

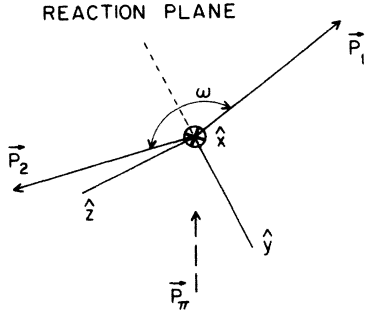


FIG. 3. The coordinate system used to monitor the alignment and measurement errors of our apparatus. The \hat{x} direction is vertically downward and all momentum vectors, \mathbf{P}_1 and \mathbf{P}_2 of the two protons and \mathbf{P}_π , are projected onto the horizontal y - z plane. The \hat{y} direction bisects the angle in the horizontal plane between the two protons and its direction varies with each event.

ordinate is in the upward vertical direction. The \hat{y} axis is the horizontal line bisecting the opening angle between the two proton momenta. The \hat{z} direction is $\hat{x} \otimes \hat{y}$. Figure 4 shows the measured missing momentum spectrum from a $\pi^+d \rightarrow pp$ run along with its Monte Carlo simulation. The missing momentum, $\mathbf{P}_\pi - \mathbf{P}_1 - \mathbf{P}_2$, according to momentum conservation should be zero for this two-body final state. The finite widths of the distributions observed are consistent with the expected experimental uncertainties. In Fig. 4(a) the P_x distribution is centered about zero, indicating proper vertical alignment of the beam spot and the wire chambers. The width of the distribution is well reproduced with the Monte Carlo code using the measurement errors quoted earlier. The missing momentum along the \hat{y} direction is shown in Fig. 4(b). Since the \hat{y} direction is nearly perpendicular to each proton's momentum, the corresponding missing momentum distribution, P_y , monitors the horizontal alignment and mea-

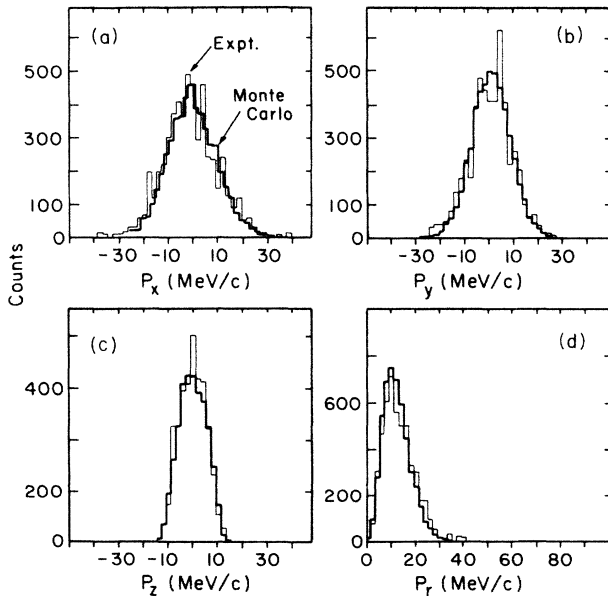


FIG. 4. The missing momentum distributions, $\mathbf{P}_\pi - \mathbf{P}_1 - \mathbf{P}_2$, calculated from the $\pi^+d \rightarrow p + p$ data, and compared with the Monte Carlo simulation (heavy line). (a) vertical direction; (b) horizontal direction, bisecting the proton's opening angle; (c) $\hat{x} \otimes \hat{y}$ direction; (d) total missing momentum.

surement errors of the wire chambers. The missing momentum P_z , which is nearly parallel or antiparallel to each proton's momentum, is shown in Fig. 4(c). If the energy calibration of one of the spectrometers was too high or low the P_z distribution would not be centered. The major contribution to the width of the P_z distribution is the variation of the proton's energy losses with the depth of the reaction vertex in the target. The radial distribution shown in Fig. 4(d) includes the factor P_R^2 from the Jacobian and is therefore not peaked at zero. Other distributions from the $\pi^+d \rightarrow pp$ data were also examined to monitor further the apparatus and showed similar high-quality results.

Another important purpose of the $\pi^+d \rightarrow pp$ measurement was to establish an absolute cross section scale. Because the positions of the spectrometers were occasionally changed, many runs had different detector solid angles. The front faces of the spectrometers had varying distances of 20 to 38 cm from the target. The two ionization chambers monitoring the beam flux remained consistent with each other to within one percent and the cross sections obtained from these different $\pi^+d \rightarrow pp$ runs agreed within a standard deviation of 2.5%.

IV. MONTE CARLO SIMULATION OF THE DATA

Never before in a $A(\pi^+,pp)B$ reaction have well-defined absolute triple-differential cross sections for $A > 3$ been obtained. The extraction of these cross sections requires a careful mapping of the detection efficiency over the full phase-space acceptance of the detectors. This is especially important in the current measurement where the beam spot on the target is large and the faces of the detectors are small. For this purpose, a Monte Carlo code was developed which simulates every important feature of the experiment, including energy straggling, Moliere scattering, and measurement errors. The Monte Carlo code uses the known $\pi^+d \rightarrow pp$ single-differential cross section to obtain the ${}^6,7\text{Li}(\pi^+,pp)$ triple-differential cross sections in a way that is described below.

A typical-differential cross section is expressed as:

$$\frac{d^3\sigma}{dE_1 d\Omega_1 d\Omega_2} = \frac{1}{(2\pi)^5} \frac{E_\pi E_1 E_2 k_1 k_2}{k_\pi [1 - (\beta_R \cdot \beta_2)/\beta_2^2]} |T|^2, \quad (1)$$

where the kinematic factor includes energies, wave numbers, and velocities of the two protons (subscripts 1 and 2) and the recoiling residual nucleus (subscript R). The transition matrix, T , is sensitive to the initial and final wave function of Li and He, respectively, and the precise nature of the reaction mechanism. Since there are three particles in the final state, nine coordinates are needed to specify the kinematics of each event, reduced to five by conservation of energy and momentum. The Monte Carlo code uses the five variables: \mathbf{P}_R , the momentum of the recoiling nucleus, and θ_1, ϕ_1 —the angles of one of the two protons. The angles, θ_1, ϕ_1 , are defined as the angles between one of the protons and the incident pion momentum direction with ϕ_1 as the azimuthal angle. These variables are chosen for reasons which simplify the data analysis. The angles θ_1 and ϕ_1 are chosen because they are constrained to a small range of values during a single experi-

mental run. The T matrix is expected to depend strongly upon the recoil momentum, $\mathbf{P}_R = \mathbf{P}_\pi - \mathbf{P}_1 - \mathbf{P}_2$. In the impulse approximation and quasideuteron model, \mathbf{P}_R is also the total momentum of the pair of nucleons on which the pion is absorbed. The goal of the Monte Carlo code is to find the ${}^6,7\text{Li}(\pi^+, \text{pp}){}^4,5\text{He}$ T -matrix dependence on four of the above five variables. The T matrix should be independent of ϕ_1 due to cylindrical symmetry. The advantage of using a procedure involving a T matrix is that it succinctly summarizes the information contained in the five-dimensional space, which would be hard to display graphically.

It was found that a choice of $|T(\theta_1, \mathbf{P}_R)|^2$ based on the quasideuteron model successfully described the experimental distributions of several transitions. In this model the pion interacts with a (pn) pair which is taken to be an internal state of 3S_1 , the quantum numbers of the deuteron. A general description of this form of the T matrix is given in Ref. 11. This successful functional form is

$$|T|^2 = f(P_R)[1 + a_2 \mathcal{P}_2(\cos\theta'_1)], \quad (2)$$

where P_R is the momentum of the residual nucleus and θ'_1 is the proton polar angle in the center-of-mass frame of the two protons; $f(P_R)$ is expressed in the laboratory system because the target is at rest in the laboratory system. In the quasideuteron model $f(P_R)$ is a form factor describing the motion of the quasideuteron with respect to the core which in plane wave Born approximation is the absolute square of the momentum wave function for the center of mass of a (pn) pair assumed to exist as a deuteron in the lithium nucleus. The second term in the T matrix is identified as the angular dependence of the elementary $\pi^+ + (\text{pn}) \rightarrow \text{p} + \text{p}$ process. For real deuterons the $\pi^+ \text{d} \rightarrow \text{pp}$ reaction at 60 MeV has an angular distribution given by $[1 + 1.09 \times \mathcal{P}_2(\cos\theta'_1)]$.

The Monte Carlo calculation begins by simulating pions incident on the target. Values of the known spatial, angular divergence, and momentum distributions of the beam are chosen randomly. The $(\pi^+ \text{pp})$ reaction is assumed to take place and one proton, p_1 , is assumed to go toward spectrometer 1. The direction of this proton is chosen randomly within the solid angle, Ω_1 . All events, regardless of where they occur on the target, are chosen randomly within this solid angle of fixed size. However, the centroid of the solid angle changes with the target impact coordinates so that it always points to the center of the detector. The proton then undergoes Moliere scattering in the target. Before proceeding with the proton it is necessary to know its energy, which can be calculated if \mathbf{P}_R is known. Therefore, an early step in the Monte Carlo simulation is to randomly choose points from the distribution for the recoil momentum P_R using the recoil momentum distribution $f(P_R)$. The cross section is assumed to be isotropic in θ_R and ϕ_R except for a known phase space factor by which each event is weighted. After \mathbf{P}_R for an event is specified, the mass of the residual nucleus is selected—either by a single state in the residual nucleus or by randomly choosing values from a series of unresolved states using spectra from the data analysis as an input distribution. At this point all remaining kinematic variables are determined by conservation laws. Both proton trajec-

tories are then examined to decide whether they stop in the detectors. Moliere scattering, range straggling, and nuclear reactions in the detectors are included in the calculation.

If both protons stop in a spectrometer, then measurement errors are assigned to the kinematic variables. The resulting distributions of the Monte Carlo detected events are then compared to the distributions obtained from the real data analysis. The data analysis must by necessity use the central-ray beam momentum and energy to calculate missing momentum and missing mass because the pion four-momentum is not measured event by event. The functional form of $f(P_R)$, and the a_2 parameter in the T matrix [Eq. (2)] are adjusted until all experimental distributions of a particular transition are reproduced using the Monte Carlo simulation.

After the T matrix is adjusted to reproduce the data for a particular transition, it can be normalized using the known $\pi^+ \text{d} \rightarrow \text{pp}$ cross sections at 59.4 MeV,

$$d\sigma/d\Omega_1 = (6.85/2\pi)[1 + 1.09 \mathcal{P}_2(\cos\theta'_1)] \text{ mb/sr},$$

measured in the center-of-mass frame. The T matrix normalization procedure takes the experimentally measured yield for the transition and divides it by the integrated beam, target thickness, computer live time, the simulated solid angle, Ω_1 , and the corresponding average Monte Carlo detection efficiency. The resulting quotient is proportional to a single-differential cross section. Since the $\pi^+ \text{d} \rightarrow \text{pp}$ reaction cross section is known, the constant of proportionality is obtained from the $\pi^+ \text{d} \rightarrow \text{pp}$ data and its Monte Carlo simulation efficiency. This constant of proportionality can then be used to get the single-differential cross section of any $\text{Li}(\pi^+, \text{pp})$ transition. Once the absolute value of a partial-differential cross section is known, then it is possible to normalize the T matrix uniquely.

An advantage of using this T -matrix formalism to extract cross sections is that it is known how the single-differential cross section, $d\sigma/d\Omega_1$, is varying over the solid angle, Ω_1 , of the Monte Carlo simulation and this variation is accounted for in the normalization procedure. This is important because the large beam position spread on target results in a large spread ($\pm 12^\circ$) in θ_1 .

V. THE ${}^6\text{Li}(\pi^+, \text{pp}){}^4\text{He}$ SPECTRA

All of the ${}^6\text{Li}(\pi^+, \text{pp}){}^4\text{He}$ data were collected with central detector angles of 60° and 102.7° , which are proton angles satisfying the $\pi^+ \text{d} \rightarrow \text{pp}$ kinematics. Missing-mass spectra for recoil momentum both less than and greater than 100 MeV/c are shown in Fig. 5. The energy resolution, determined primarily by energy straggling in the target, is about 1.8 MeV FWHM. The ${}^4\text{He}$ ground state transition dominates the spectrum for recoil momentum less than 100 MeV/c. For recoil momentum greater than 100 MeV/c more of the yield is in the excited state region between 20 and 40 MeV. There are events in Fig. 5 between the ground state and 20 MeV excitation which are due to the ${}^7\text{Li}$ impurity in the ${}^6\text{Li}$ target. Part of the yield at energies above 20 MeV excitation is due to four, five, and six particle-final states in the ${}^6\text{Li}(\pi^+, \text{pp})$ reaction.

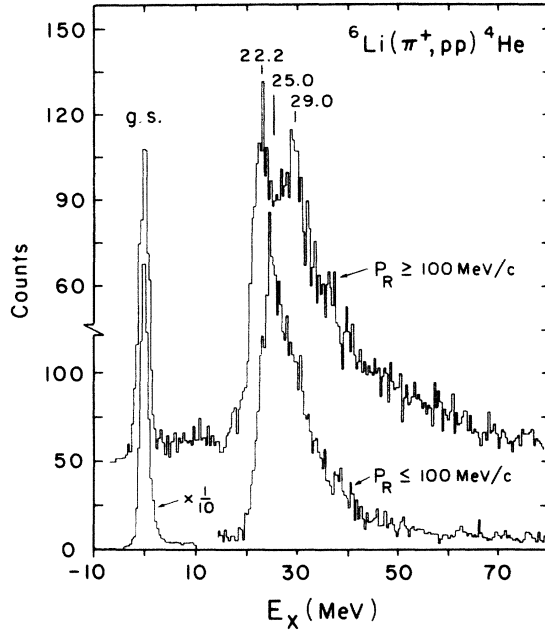


FIG 5. The ${}^6\text{Li}(\pi^+, pp){}^4\text{He}$ spectra at $T_\pi = 59.4$ MeV. The data are separated into two spectra with recoil momentum less than and greater than 100 MeV/c. The ground state peak only for events having $P_R \leq 100$ MeV/c is times $\frac{1}{10}$. The lower scale refers to the spectra corresponding to $P_R \leq 100$ MeV/c. The excitation energies corresponding to the centroids of the observed peaks are indicated.

This is because ${}^4\text{He}$ is unbound to proton decay above 19.8 MeV excitation and can completely separate into two neutrons and two protons above 28.3 MeV.

Superimposed on the continuum above 20 MeV is an indication of three strongly populated states in ${}^4\text{He}$ at excitation energies of 22.2 ± 0.4 , 25.0 ± 0.4 , and 29.0 ± 0.4 MeV. The 25.0 MeV state dominates the spectrum of events with recoil momentum less than 100 MeV/c, whereas the other two states dominate the spectrum of events with recoil momentum greater than 100 MeV/c. Of these three states, the two strongest states at 22.2 and 25.0 MeV agree with the two strongest excited states seen in the ${}^6\text{Li}(d, \alpha){}^4\text{He}$ reaction at excitation energies of 21.9 and 25.5 MeV.¹⁰ There is weak evidence for two other excited states in the ${}^6\text{Li}(d, \alpha){}^4\text{He}$ data at 28.5 and 31.8 MeV excitation and have widths greater than 5.0 MeV. The similarity between the (π^+, pp) and (d, α) spectra is evident in other nuclei. The four strongest states seen in the ${}^{16}\text{O}(d, \alpha){}^{14}\text{N}$ reaction¹¹ are also the four strongest states seen in the ${}^{16}\text{O}(\pi^+, pp){}^{14}\text{N}$ reaction.¹² This similarity between the two reactions suggests that the (π^+, pp) reaction

is primarily selecting a (pn) pair in a $T=0$, 3S_1 configuration.

The level of 22.2 ± 0.4 MeV is thought to be the known 2^- level at 22.1 MeV. This state has a s^3p^1 configuration; therefore, the transition to this state involves the removal of a $1s$ and $1p$ nucleon from the ${}^6\text{Li}$ target. This is consistent with the state's higher yield at large recoil momentum.

This 2^- level is not expected to be strongly populated in the ${}^6\text{Li}(\pi^+, pp)$ reaction because it must involve nucleons from two different shells.^{13,14} While previous $(\pi, 2N)$ data⁴ indicate the suppression of absorption on nucleons in different shells, recent measurements^{15,16} comparing absorption cross sections from ${}^{18}\text{O}$ and ${}^{16}\text{O}$ and a theoretical calculation¹⁷ suggest otherwise. The measurement from Ref. 14 indicates that the total π^+ absorption cross section at $T_\pi = 165$ MeV on ${}^{18}\text{O}$ is 17% larger than the total absorption cross section on ${}^{16}\text{O}$. The significant population of the 2^- state provides more evidence that the pion is also absorbed on nucleons in different shells.

The remaining two excited states in the ${}^6\text{Li}(\pi^+, pp){}^4\text{He}$ spectra are believed to be positive parity states involving the removal of two $1s$ nucleons. The state at 25.0 MeV is identified with the state in the ${}^6\text{Li}(d, \alpha){}^4\text{He}$ reaction at 25.5 MeV and is a known state of $J^\pi = 0^+$ or 1^+ .

VI. THE ${}^6\text{Li}(\pi^+, pp){}^4\text{He}$ T MATRICES

The recoil momentum distribution $f(P_R)$ in Eq. (2) for the ${}^6\text{Li}(\pi^+, pp){}^4\text{He}$ ground state transition is shown in Fig. 6. The measured half-width at half maximum (HWHM) is 36 ± 4 MeV/c. This compares favorably with the HWHM measured to be 34 ± 1.5 MeV/c in the ${}^6\text{Li}(e, e'\alpha)$ reaction,¹⁸ 32 ± 1 MeV/c in the ${}^6\text{Li}(e, e'd)$ reaction,¹⁸ and 43 MeV/c in the ${}^6\text{Li}(p, pd){}^4\text{He}$ reaction at $T_p = 670$ MeV.¹⁹ The value obtained from the ${}^6\text{Li}(\pi^-, nn){}^4\text{He}$ experiment⁴ is ~ 45 MeV/c which is consistent with this measurement within the errors of the two experiments.

If fine detail exists in the form factors, it will be partially washed out by the poor recoil momentum resolution of our system. Figure 4 gives a good indication of the recoil momentum resolution at small values of P_R . The resolution improves significantly as P_R increases. Since the only model dependence in the extraction of $f(P_R)$ is the unfolding of the errors from the experimental distributions, it is valuable to examine these errors in more detail. In Fig. 7 we plot (solid line) a theoretical ${}^6\text{Li}-{}^4\text{He} + d$ form factor calculated by Lehman.²⁰ The so-called "experimental points" in both Figs. 6 and 7 are defined as

$$\text{"experimental points"} = \text{data events}(P_R) \frac{f(P_R)}{\text{Monte Carlo}(P_R)}. \quad (3)$$

The input form factor, $f(P_R)$, is divided by the output distribution from the Monte Carlo code in the above expression.

If there were no measurement uncertainties in our experiment, the factor multiplying the data events would simply be the correction for the phase space acceptance of

our detector. However because of the model dependence of the error simulation in the Monte Carlo code the data points in Figs. 6 and 7 for the ${}^4\text{He}$ ground state transition are slightly different. In Fig. 6 the form factor which best fits the data was used as input to the Monte Carlo code whereas in Fig. 7 the Lehman form factor was used. This

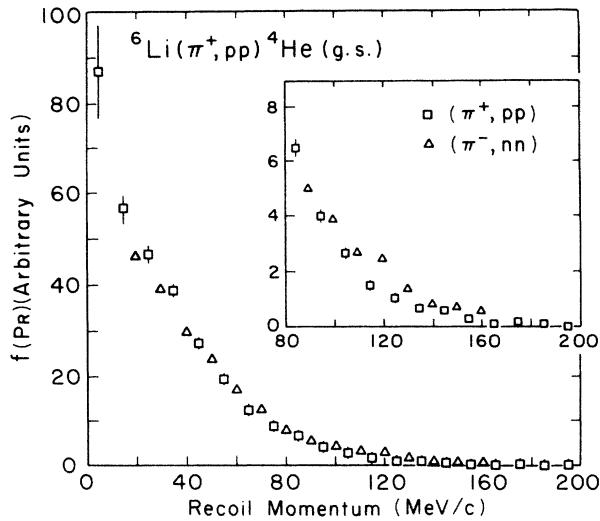


FIG. 6. The recoil momentum distribution, $f(P_R)$, for the transition to the ${}^4\text{He}$ ground state, obtained from the ${}^6\text{Li}(\pi^+, pp){}^4\text{He}$ data and from earlier ${}^6\text{Li}(\pi^-, nn){}^4\text{He}$ data (Ref. 3). The inset is an enlargement of the high momentum region. Error bars give the statistical errors.

theoretical form factor from Lehman has a narrow minimum at 140 MeV/c. The Monte Carlo code simulates the experimental errors and smears this minimum over a large range of P_R values. If the minimum at 140 MeV/c in the Monte Carlo output is severely washed out by errors, then the experimental points as defined by Eq. (3) will follow rapid changes in the input form factor giving a model dependent data reduction. Fortunately this is not the case. The experimental points remain high near 140 MeV/c and are in disagreement with the theoretical form factor. This test gives us confidence that the extracted form factor is not strongly dependent upon the initial form factor used in the Monte Carlo simulation.

Total experimental yields in the excitation regions

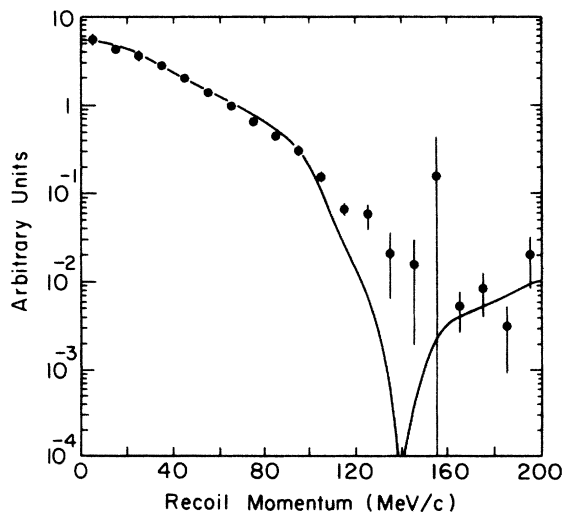


FIG. 7. Another version of the form factor for the ${}^6\text{Li}(\pi^+, pp){}^4\text{He}$ ground state transition. See the text for an explanation. The solid line is Lehman's theoretical form factor from Ref. 20.

20–23 MeV, 23–28 MeV, and 29–35 MeV were studied to obtain an average recoil momentum distribution for each region. These are shown in Fig. 8. All three excitation regions share a common continuum which is populated primarily by the pion absorbing on two $1s$ nucleons. This may be responsible for the similar shapes of the distributions.

The enhancement at low recoil momentum of the ${}^4\text{He}$ ground state transition indicates an angular momentum transfer, $L=0$. Similarly the 25 MeV transition appears to be dominated by an $L=0$ component. The recoil momentum distributions for the 22.2 and 29.0 MeV transitions are more pronounced at large recoil momentum, indicating an important nonzero angular momentum component. The distribution for the 22.2 MeV transition has a sizable yield in the 100 to 200 MeV/c region indicating an $L=1$ transition consistent with the removal of a $1s$ and $1p$ nucleon as stated before.

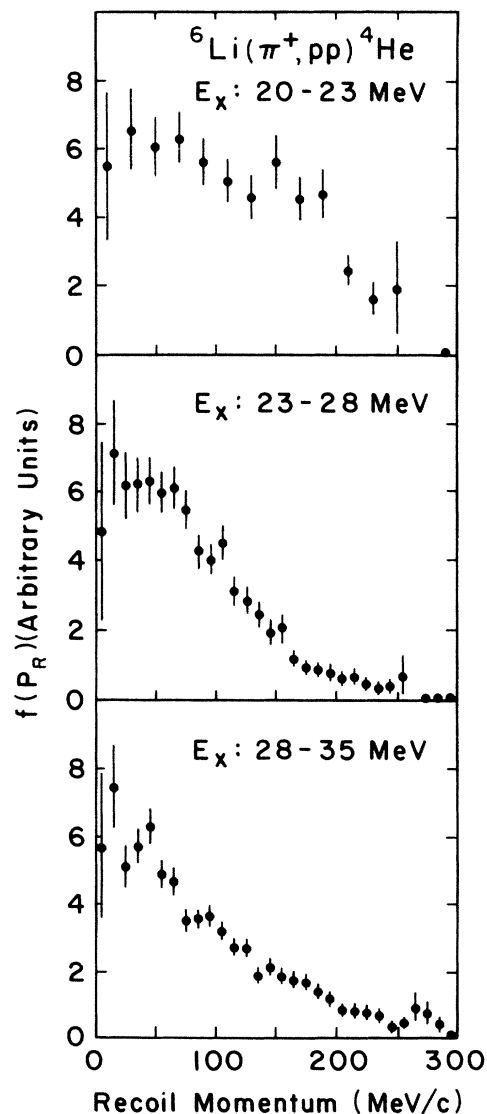


FIG. 8. The recoil momentum distribution, $f(P_R)$, for the sum of all of the ${}^6\text{Li}(\pi^+, pp){}^4\text{He}$ transitions into the (a) 20–23 MeV excitation region, (b) 23–28 MeV excitation region, (c) 28–35 MeV excitation region. The errors are statistical.

The 29.0 MeV transition is better seen in the missing mass spectra for recoil momentum greater than 100 MeV/c. Although no recoil momentum distribution was extracted for this transition, the data appear to be more consistent with an $L=1$ or $L=2$ transition than with an $L=0$ transition.

The T matrices for all of the transitions could be described using only two variables, P_R and θ_1 . A typical example of the recoil isotropy is shown for the ${}^4\text{He}$ ground state transition in Fig. 9. The recoil angle, θ_R , is defined as $\cos\theta_R = \hat{P}_R \cdot \hat{P}_\pi$. The errors are statistical. The Monte Carlo simulation reproduces the θ_R distribution successfully without any θ_R or ϕ_R dependence in the T matrix. The absence of any sizable θ_R or ϕ_R dependence in the T matrix is in sharp contrast to the strong θ_R, ϕ_R

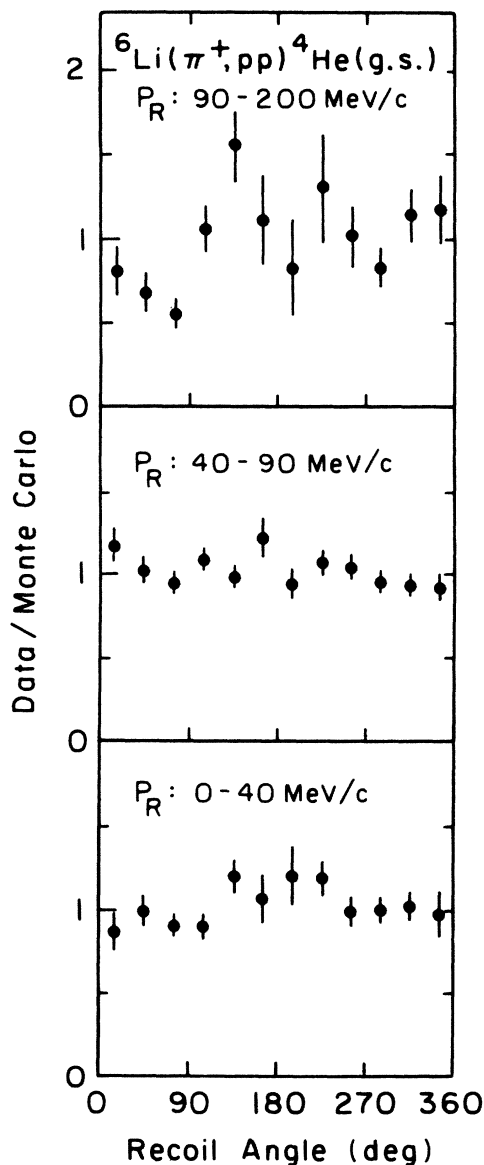


FIG. 9. Plots of the recoil angle, θ_R , distribution of the ${}^6\text{Li}(\pi^+, \text{pp}){}^4\text{He}$ ground state data divided by the Monte Carlo simulation in which the functional form of the T matrix is Eq. (2). The plots are shown for different values of recoil momentum. The errors are statistical.

dependence seen in the ${}^{16}\text{O}(\pi^+, \text{pp}){}^{14}\text{N}$ reaction.¹²

The dependence of the T matrix upon the remaining kinematic variable, θ'_1 , is assumed to be the same as the θ_1 dependence in the elementary $\pi + d \rightarrow p + p$ reaction. Based on this assumption, a_2 in Eq. (2) was chosen to be 1.09. This assumption could not be fully tested because of the limited range of θ'_1 values.

To summarize, the most accurate distributions are for the ${}^4\text{He}$ ground state transition, for which the T matrix is consistent with the predicted T matrix of the quasifree model where the (pn) pair have the quantum numbers of a deuteron. The T matrices for the excited state region, averaged over excitation energy, also show an isotropy in the θ_R and ϕ_R distributions. The same functional form as the ground state transition was used for these excited states, including a value of 1.09 for a_2 .

VII. THE ${}^6\text{Li}(\pi^+, \text{pp}){}^4\text{He}$ CROSS SECTIONS

Once the functional form and the magnitude of the T matrix for a particular (π^+, pp) transition is known, it can be used to calculate any single-, double-, or triple-differential cross section. A computer program, TRIDIF, was written for this purpose. Any triple-differential cross section calculated by TRIDIF within the phase space acceptance of the detectors is model independent to the extent that the T matrix used in TRIDIF was freely adjusted until it reproduced the data. Calculating any single- or double-differential cross section using TRIDIF, or a total-integrated cross section involves the extrapolation of the T matrix into unmeasured regions of phase space.

Triple-differential cross sections calculated by TRIDIF

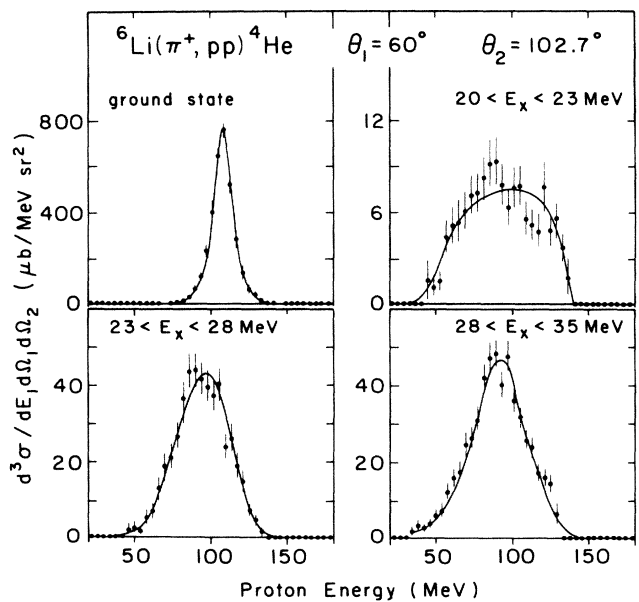


FIG. 10. The triple-differential cross sections of the transitions to the (a) ground state, (b) 20–23 MeV excitation region, (c) 23–28 MeV excitation region, (d) 28–35 MeV excitation region. In all cases, $\theta_1=60^\circ$, $\phi_1=270^\circ$, $\theta_2=102.7^\circ$, $\phi_2=90^\circ$. The data points are described in the text. The solid line is the TRIDIF calculation including recoil momenta up to 300 MeV/c.

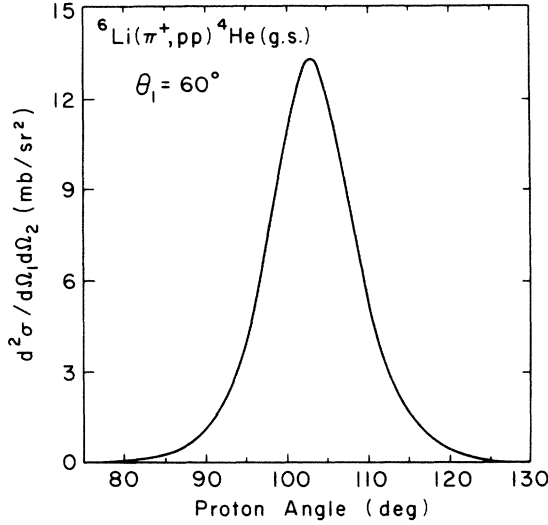


FIG. 11. A calculated double-differential cross section for the ${}^6\text{Li}(\pi^+,pp){}^4\text{He}$ ground state transition plotted against θ_2 . The calculation is an extrapolation of the real data. The fixed angles are $\theta_1=60^\circ$, $\phi_1=270^\circ$, and $\theta_2=90^\circ$.

are shown for the central value of the detector angles: $(\theta_1, \theta_2)=(60^\circ, 102.7^\circ)$ in Fig. 10. The “experimental” points in this figure show the statistical errors from the data and the Monte Carlo simulation. These “data” points are

$$\text{“data points”} = \frac{\text{data events}(E_1)}{\text{Monte Carlo}(E_1)} \frac{d^3\sigma(\text{TRIDIF})}{d\Omega_1 d\Omega_2 dE_1}, \quad (4)$$

where the same T matrix was used in both the TRIDIF and the Monte Carlo code. The degree to which the TRIDIF calculation goes through the data points indicates how well the Monte Carlo code is replacing the data. The proton energy distributions are well reproduced by the Monte Carlo simulation. Only the statistical errors are shown in Fig. 10.

Approximately 95% of the integral of the triple-differential cross section over dE_1 is contained within the phase space acceptance of the detectors. The result of this integral gives the ${}^4\text{He}$ ground state’s double-differential cross section shown in Fig. 11. No data points are shown because it is not an actual measurement but rather, an extrapolation based on the present data.

The double-differential cross sections are integrated over $d\Omega_2$ to get the single-differential cross sections, $d\sigma/d\Omega_1$, shown in Table I. The integral over $d\Omega_2$ in-

volves a major extrapolation of the T matrix. About 25% of the ground state single-differential cross section and 10% of the excited state single-differential cross section is contained within the solid angle, Ω_2 , of the second spectrometer. Much of the extrapolation into the unmeasured region involves a knowledge of $f(P_R)$ at large values of recoil momentum. In Table I the single-differential cross sections are given for different cutoff values of recoil momentum. Above these cutoff momenta, the recoil momentum (Figs. 6 and 8) is set equal to zero. Table I shows that 96% of the cross section to the ${}^4\text{He}$ ground state is in the region of recoil momentum below 150 MeV/c. In contrast, the excited state region between 28 and 35 MeV excitation has 28% of the cross section coming from events with missing momentum greater than 200 MeV/c. The statistical error on these cross sections are a few percent in all cases.

The single-differential cross sections are given for different cutoff values of recoil momentum for several reasons. The angular dependence of $f(P_R)$ is not known as accurately at large recoil momentum. The data is restricted to a very narrow range of θ_R and ϕ_R values at large recoil momentum making it difficult to accurately verify the assumption that the T matrix is isotropic in these variables. If there are n particles in the final state the recoil momentum is the sum of the momenta of the $(n-2)$ undetected particles. According to phase space distributions, most of the yield for final states with $n \geq 4$ will be in the region of missing momentum greater than 200 MeV/c. The different cutoff momenta values can help to interpret the contamination due to four-, five-, and six-body final states, and to select out the ${}^6\text{Li}(\pi^+,pp){}^4\text{He}$ three-body component from the data. The definition of three-body components used includes transitions to unbound states of ${}^4\text{He}$ which later decay into two or more particles. The $n \geq 4$ component is assumed not to involve an intermediate ${}^4\text{He}$ state.

Dividing the single differential cross section for the ${}^4\text{He}$ ground state transition by the $\pi^+d \rightarrow pp$ cross section, which was also measured with this apparatus, gives 0.98 ± 0.02 . This result, which indicates that the ground state cross section is almost identical to the elementary $\pi^+d \rightarrow pp$ cross section, gives more evidence supporting the quasideuteron model. It is not surprising that the quasideuteron mechanism describes this transition well because the quasideuteron cluster (p -shell nucleons) which is removed from ${}^6\text{Li}$ is only bound by 1.47 MeV.

The near equality of the ${}^6\text{Li}(\pi^+,pp){}^4\text{He}$ ground state

TABLE I. $d\sigma/d\Omega_1$ ($\mu\text{b}/\text{sr}$) for ${}^6\text{Li}(\pi^+,pp){}^5\text{He}$ (at $T_\pi=59.4$ MeV, $\theta_1=60^\circ$). Values show statistical errors and are based upon an extrapolation of a 25% (or 10%) measurement of the total yield.

Excitation energy (MeV)	Upper cutoff in recoil momentum (MeV/c)			
	150	200	250	300
0.0	775 ± 18	805 ± 19	805 ± 19	805 ± 19
20→23	118 ± 5	243 ± 1	346 ± 15	381 ± 17
23→28	388 ± 11	552 ± 16	664 ± 19	692 ± 21
28→35	367 ± 10	745 ± 20	937 ± 27	1102 ± 36
0→35	1650 ± 24	2350 ± 33	2750 ± 41	2980 ± 49

cross section and the $\pi^+d \rightarrow pp$ single differential cross section has also been observed in the work of Favier *et al.*¹ As part of the same experimental program²¹ the ratio of the yields of the ${}^6\text{Li}(\pi^+,pp){}^4\text{He}$ ground state and the $\pi^+d \rightarrow pp$ reaction were found to be constant at a value of 0.91 ± 1 for incident pion energies varying between 50 and 275 MeV. The same ratio for the excitation region between 20 and 50 MeV remained constant at about 1.6. The corresponding number for this experiment is ~ 2 . The numbers 0.91 and 1.6 should be considered as lower limits because their data only covers a finite region of the available phase space, however their detectors each covered a large solid angle, of about 0.25 steradians. This is a significant result, indicating that both the magnitude and the strong energy dependence for the ground state, as well as the energy dependence for the excited state region, are similar for pion absorption on both deuterons and ${}^6\text{Li}$.

The agreement of the cross sections of Favier's experiment and the single-differential cross sections obtained by extrapolation in this experiment is an indication that the T matrices for the ground state transition and excited state transitions are a reasonable representation of the reaction. The ${}^6\text{Li}(\pi^+,pp){}^4\text{He}$ ground state and $\pi^+d \rightarrow pp$ cross sections appear to have nearly the same magnitude and the same dependence upon pion energy and proton angle. The quasideuteron model appears to work well.

If the quasideuteron model prediction for the a_2 parameter is correct, then the integration of the single-differential cross sections over $d\Omega_1$ should give reliable total integrated cross sections. The resulting integrated cross sections, obtained by extrapolating the T matrices over the full phase space, are

$$\sigma[{}^6\text{Li}(\pi^+,pp){}^4\text{He}(\text{g.s.})] = 6.7 \text{ mb},$$

$$\sigma[{}^6\text{Li}(\pi^+,pp){}^4\text{He}(20-35 \text{ MeV})] = 13.7 \text{ mb}.$$

The sum of these cross sections (~ 20 mb) should be compared to the total absorption cross section of 60 MeV π^+ on ${}^6\text{Li}$. When the pion absorption data at 50 (Ref. 22) and 85 MeV,²³ are interpolated to 60 MeV, a total absorption cross section of 36 ± 10 mb is obtained. This interpolation of the data indicates that the ${}^6\text{Li}(\pi^+,pp){}^4\text{He}$ reaction takes about 60 percent of the total π^+ absorption cross section at $T_\pi = 60$ MeV.

The π^+ total absorption cross section for ${}^6\text{Li}$ increases much faster with pion energy than the elementary $\pi^+ + d \rightarrow p + p$ or ${}^6\text{Li}(\pi^+,pp)$ reactions. At $T_\pi = 60$ MeV the ratio of the π^+ absorption cross sections on ${}^6\text{Li}$ to that of ${}^2\text{H}$ is about 5.5 whereas at 160 MeV it is about 11.^{10,15,23} If the ${}^6\text{Li}(\pi^+,pp){}^4\text{He}$ cross section²¹ has the same energy dependence and angular dependence as the $\pi^+d \rightarrow pp$ cross section, the percentage of the total absorption cross section feeding the ${}^6\text{Li}(\pi^+,pp){}^4\text{He}$ channels is falling from approximately 60% to 30% as the pion energy increases from 60 up to 160 MeV.

VIII. A COMPARISON WITH THE ${}^6\text{Li}(\pi^+,p)$ INCLUSIVE CROSS SECTIONS

A T -matrix formula based on a modified quasifree absorption model has been used to parametrize our data. To

test the predictive powers of the model, the T matrices that describe the ${}^6\text{Li}(\pi^+,pp){}^4\text{He}$ data are extrapolated in both angle and incident pion energy to calculate the ${}^6\text{Li}(\pi^+,p)$ inclusive cross sections using the computer code TRIDIF. These results are compared with the inclusive pion absorption data on ${}^6\text{Li}$ of McKeown *et al.*⁶

These ${}^6\text{Li}(\pi^+,p)$ inclusive cross sections have been measured at $T_\pi = 160$ and 220 MeV for which the yield at large proton energy (greater than T_π) is primarily from pion absorption processes in order to obtain the necessary kinetic energy. The lighter nuclei (${}^{12}\text{C}$, ${}^6\text{Li}$, and ${}^4\text{He}$) measured at these pion energies all show a peak centered at the proton energy expected from the elementary absorption reaction $\pi + 2N \rightarrow 2N$. This suggests that the ${}^6\text{Li}(\pi^+,p){}^4\text{He}$ reaction may be the dominant part of the inclusive cross section at these proton energies.

Double-differential cross sections $d^2\sigma/dE_1 d\Omega_1$ at 30° , $T_\pi = 160$ MeV and $T_\pi = 220$ MeV were calculated from the measured T matrices for the ${}^6\text{Li}(\pi^+,pp){}^4\text{He}$ reaction (Sec. VI) using the computer code, TRIDIF. The magnitudes of the resulting cross sections were renormalized based on a quasideuteron model.

Bressani *et al.*²¹ have measured the ${}^6\text{Li}(\pi^+,pp){}^4\text{He}$ differential cross section at a single angle (90° in the pp center of mass) and over a wide range of incident pion energies. The cross sections were found to have a dependence on the incident pion energy similar to that of the $\pi^+d \rightarrow pp$ reaction from 50 to 275 MeV. Assuming that the (π^+,pp) reaction has the same energy and angle dependence as that of the $\pi^+d \rightarrow pp$ reaction, the single-differential cross sections in the laboratory frame at 30° , 160 MeV and 30° , 220 MeV are, respectively, 4.6 and 2.4 times the single-differential cross section at 60° , 59.4 MeV.

The sum of the TRIDIF double-differential cross sections extrapolated from the measured ${}^6\text{Li}(\pi^+,pp){}^4\text{He}$ reaction for the ground state and excited states up to 35 MeV excitation are compared with the measured inclusive ${}^6\text{Li}(\pi^+,p)$ double-differential cross sections at each energy in Fig. 12. The TRIDIF calculations use recoil momentum distributions taken out to 200 and 300 MeV/ c . Contam-

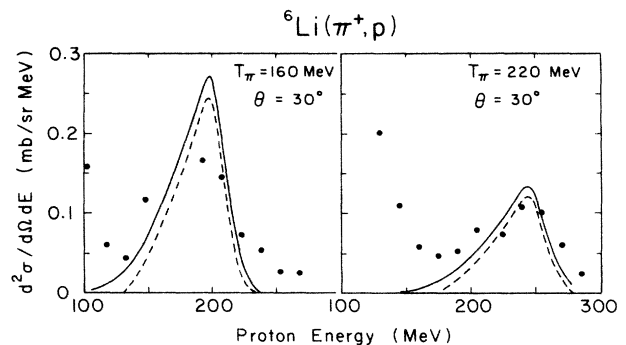


FIG. 12. The double-differential cross sections of the inclusive ${}^6\text{Li}(\pi^+,p)$ reaction (Ref. 6) compared to the extrapolation of the measured ${}^6\text{Li}(\pi^+,pp){}^4\text{He}$ data using the computer code, TRIDIF. The solid and dashed lines are the TRIDIF calculations using recoil momenta up to 300 and 200 MeV/ c , respectively.

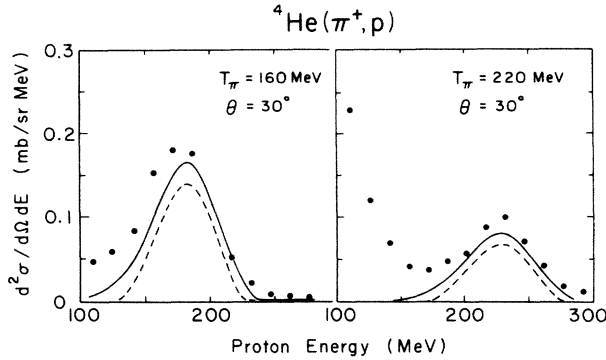


FIG. 13. The double-differential cross sections of the inclusive ${}^4\text{He}(\pi^+, p)$ reaction (Ref. 6) compared to the TRIDIF extrapolation of the ${}^6\text{Li}(\pi^+, pp){}^4\text{He}$ data between 20 and 35 MeV excitation. The solid and dashed lines are the cutoffs in the recoil momentum of 300 and 200 MeV/c, respectively.

ination from four-, five-, and six-body events in the data at 59.4 MeV is minimized by cutting off these distributions at 200 MeV/c; those calculations are shown in Fig. 12 as the dashed lines.

The inclusive ${}^6\text{Li}(\pi^+, p)$ cross section data at 30° and $T_\pi = 160$ and 220 MeV shown in Fig. 12 indicate a peak at a proton energy of 200 and 240 MeV, respectively. The TRIDIF calculation predicts a narrow peak at 200 MeV, however it overshoots the data by roughly 50% at $T_\pi = 160$ MeV and approximately agrees with the data at 220 MeV (Fig. 12). Note that the TRIDIF calculation should only be compared to the data near the peak, since at lower proton energies other processes are expected to contribute substantially to the ${}^6\text{Li}(\pi^+, p)$ yield. At higher proton energies (235 MeV for the $T_\pi = 160$ MeV data and 280 MeV for the $T_\pi = 220$ MeV data), the ${}^6\text{Li}(\pi^+, p)d^3\text{He}$ channel may be significant.²⁴ The final states of ${}^4\text{He}$ between 20 and 35 MeV excitation from the ${}^6\text{Li}(\pi^+, pp){}^4\text{He}$ reaction, except for the 2^- state at 22.1 MeV (see Sec. V), should correspond to pion absorption on a (pn) pair from the s -shell nucleons of ${}^6\text{Li}$. These s -shell nucleons can often be described as an alpha cluster, therefore, the sum of ${}^6\text{Li}(\pi^+, pp){}^4\text{He}$ cross sections between 20 and 35 MeV should be similar to the ${}^4\text{He}(\pi^+, pp){}^2\text{H}$ cross section. It is interesting to compare the measured inclusive ${}^4\text{He}(\pi^+, p)$ double-differential cross sections from Ref. 5 with the integrated ${}^6\text{Li}(\pi^+, p){}^4\text{He}$ double differential cross sections for these final states. The TRIDIF calculation for this excited state region is compared to the inclusive ${}^4\text{He}(\pi^+, p)$ cross sections in Fig. 13. Here the calculation based on the integrated ${}^6\text{Li}(\pi^+, p){}^4\text{He}$ double differential cross section is in qualitative agreement ($\pm 20\%$) with the inclusive ${}^4\text{He}(\pi^+, p)$ cross section data at both proton energies.

In the four (π^+, p) inclusive spectra discussed there is qualitative agreement with the peak observed near 200 MeV, however the peak shape in the $T_\pi = 160$ MeV ${}^6\text{Li}$ case is poorly reproduced. Because the results are mixed, conclusions as to the success of the extrapolation are premature. However, with a more complete data set this type of comparison might be useful. To our knowledge, the (π^+, pp) and (π^+, p) inclusive data have never before been compared in this way.

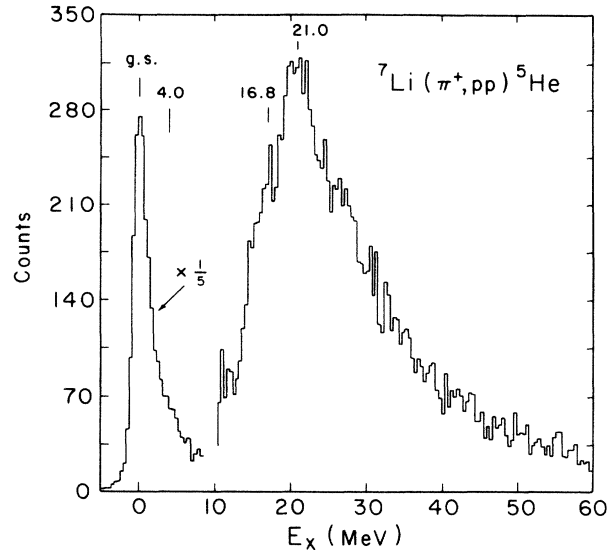


FIG. 14. A ${}^7\text{Li}(\pi^+, pp){}^5\text{He}$ spectrum at $T_\pi = 59.4$ MeV.

IX. THE ${}^7\text{Li}(\pi^+, pp){}^5\text{He}$ SPECTRA

The ${}^7\text{Li}(\pi^+, pp){}^5\text{He}$ data were collected at two pairs of detector angles ($60^\circ, 102.7^\circ$) and ($80.5^\circ, 80.5^\circ$) which each satisfy the $\pi^+ d \rightarrow pp$ kinematics. Figure 14 is a typical spectrum showing the ${}^5\text{He}$ $\frac{3}{2}^-$ ground state with a broad ($\Gamma = 4$ MeV) overlapping $\frac{1}{2}^-$ excited state at 4 MeV and a broad peak between 16 and 35 MeV excitation. In this 16 to 35 MeV excitation region one strong peak is seen at about 21 MeV with a width of about 4 MeV. This overall spectrum is very typical of ${}^5\text{He}$ spectra observed in other reactions; only a few states in ${}^5\text{He}$ have previously been identified.

The dominant peaks observed in the ${}^7\text{Li}(d, \alpha){}^5\text{He}$ reaction apart from the ${}^5\text{He}$ ground state region are two states at 20.2 and 23.8 MeV with widths of 2 and 1 MeV, respectively.²⁵ This is consistent with a 4 MeV wide peak observed here at 21 MeV in the ${}^7\text{Li}(\pi^+, pp){}^5\text{He}$ spectra with an experimental resolution of 2 MeV. The ${}^7\text{Li}(d, \alpha){}^5\text{He}$ spectra²⁵ also show a weak state at 16.7 MeV excitation which is identified as the known 16.76 MeV $\frac{3}{2}^+$ state in ${}^5\text{He}$. It is unclear if the ${}^7\text{Li}(\pi^+, pp){}^5\text{He}$ spectra show this 16.8 MeV state because there are contaminant peaks from the ${}^{16}\text{O}(\pi^+, pp){}^{14}\text{N}$ and ${}^{12}\text{C}(\pi^+, pp){}^{10}\text{B}$ reactions that would occur at about 15 MeV excitation in the ${}^7\text{Li}(\pi^+, pp){}^5\text{He}$ spectra. The ${}^7\text{Li}(\pi^+, pp){}^5\text{He}$ spectra appear similar to the ${}^7\text{Li}(d, \alpha){}^5\text{He}$ spectra, a trend also seen for the ${}^6\text{Li}$ target.

X. THE ${}^7\text{Li}(\pi^+, pp){}^5\text{He}$ T MATRICES

The ${}^5\text{He}$ $\frac{3}{2}^-$ ground state and the 4 MeV $\frac{1}{2}^-$ excited state, with its natural width of about 4 MeV, overlap each other in the ${}^7\text{Li}(\pi^+, pp){}^5\text{He}$ spectra and it is difficult to obtain separate recoil momentum distributions, $f(P_R)$, for each transition. Average distributions for the excitation regions: $-3 < E_x < 1$ MeV and $1 < E_x < 10$ MeV were obtained instead. About 90% of the yield in the first region is from the ${}^5\text{He}$ $\frac{3}{2}^-$ ground state transition and the remaining 10% is made up from half of the total yield

from the $\frac{1}{2}^-$ 4 MeV transition. The other 50% of the 4 MeV state makes up the second region. The recoil momentum distribution for the ground state region and also for the 4 MeV excitation region are shown in Fig. 15. Both distributions peak at zero recoil momentum and the HWHM in the ground state region is 61 ± 5 MeV/c and in the 4 MeV region is 83 ± 6 MeV/c. This is similar to analysis of the ${}^7\text{Li}(\pi^-, \text{nn}){}^5\text{He}$ reaction⁴ for which half-widths of about 65 and 83 MeV/c for the two regions are obtained, respectively. This is also similar to the HWHM of 63 ± 8 MeV/c obtained for the sum of these two regions in the ${}^7\text{Li}(\text{p}, \text{pd}){}^5\text{He}$ reaction.²⁶

The quasideuteron model suggests that the form factor for the 4 MeV transition should be broader than the ground state transition by only a few MeV/c due to the larger binding energy in disagreement with the data.

Another interesting feature is that $f(P_R)$ for the ground state between 160 and 240 MeV/c changes with the proton angle, θ_1 (see Fig. 15). Although the statistics are limited, at $\theta_1 = 60^\circ$ the recoil momentum distribution in this momentum region is systematically larger than the corresponding distribution at $\theta_1 = 80.5^\circ$. This behavior is not seen in the $f(P_R)$ distribution for the $1 < E_x < 10$ MeV region.

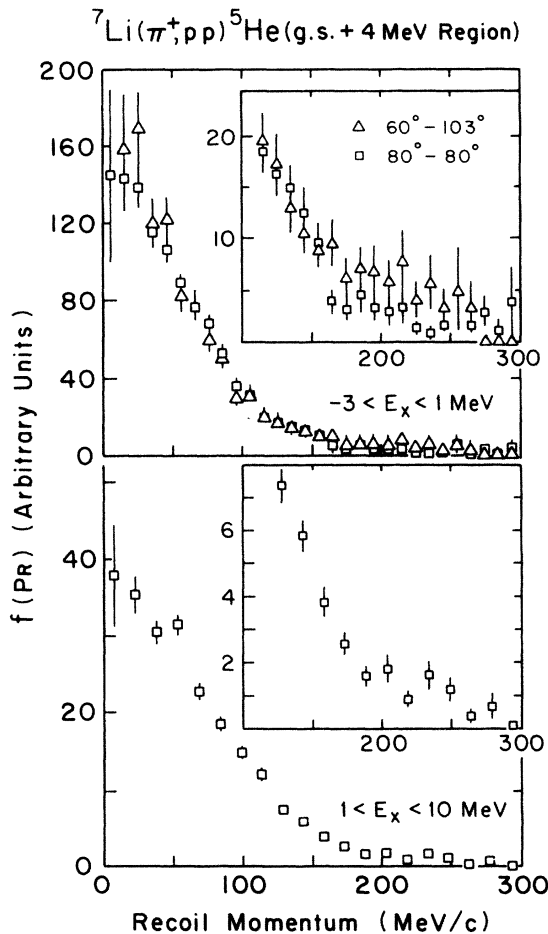


FIG. 15. The recoil momentum distributions extracted from the ${}^7\text{Li}(\pi^+, \text{pp}){}^5\text{He}$ data for the excitation energy regions of -3 to 1 MeV (top) and 1 to 10 MeV (bottom). These regions correspond to the $\frac{3}{2}^-$ ground state and $\frac{1}{2}^-$ 4 MeV state.

The recoil momentum distributions for the transitions to the higher excited state region of the ${}^7\text{Li}(\pi^+, \text{pp}){}^5\text{He}$ reaction are shown in Fig. 16. The distribution for the 16 to 19 MeV excitation region shows a similar dependence upon proton angle, θ_1 , as the ground state transition. Between recoil momenta of 150 and 230 MeV/c, $f(P_R)$ is a factor of 2 larger at $\theta_1 = 60^\circ$ than at $\theta_1 = 80.5^\circ$. This excitation region, 16 to 19 MeV, is the region most severely contaminated by ${}^{16}\text{O}(\pi^+, \text{pp})$ and ${}^{12}\text{C}(\pi^+, \text{pp})$ events due to the oxidation of the lithium target and the carbon in the plastic bag surrounding the target. However, the impurity reactions are estimated to be less than 10% of the total events and should not have any θ_1 dependence in $f(P_R)$, so that it is unlikely that the angular dependence in the recoil momentum distribution is due to contaminants.

The distributions for transitions to the 19 to 28 MeV excitation region and the 28 to 35 MeV excitation region (Fig. 16) show no variation with proton angle θ_1 . The HWHM of these $f(P_R)$ distributions is about 155 MeV/c, which is considerably larger than the HWHM of 110 MeV/c measured in the ${}^6\text{Li}(\pi^+, \text{pp}){}^4\text{He}$ reaction to states of similar excitation energy (see Sec. V). Values of the

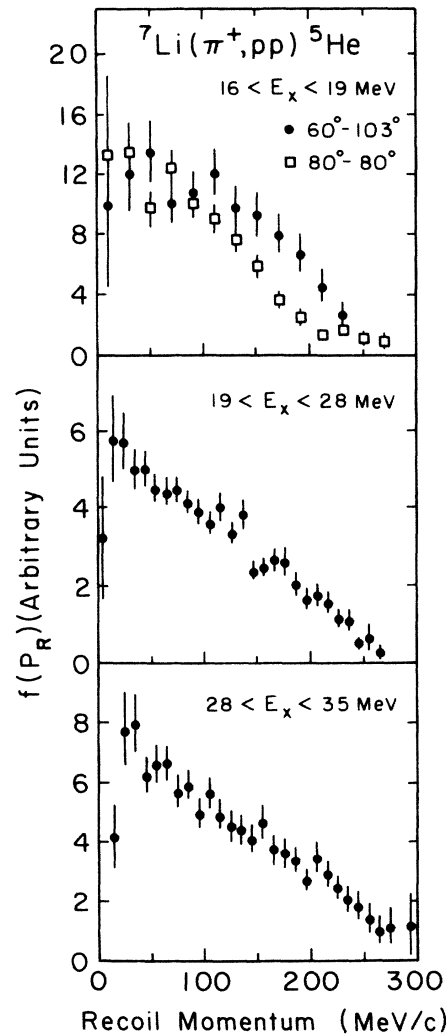


FIG. 16. The recoil momentum distributions extracted from the ${}^7\text{Li}(\pi^+, \text{pp}){}^5\text{He}$ data in the high excitation energy regions.

TABLE II. The a_2 parameter in the ${}^7\text{Li}(\pi^+, \text{pp}){}^5\text{He}$ T matrices.

Excitation energy (MeV)	Upper cutoff in recoil momentum (MeV/c)			
	150	200	250	300
-3→1	1.13±0.14	1.29±0.12	1.39±0.12	1.44±0.11
1→10	1.16±0.13	1.06±0.14	1.04±0.14	0.99±0.14
-3→10	1.14±0.12	1.18±0.11	1.24±0.11	1.19±0.11
16→19	1.37±0.18	1.55±0.17	1.57±0.17	1.55±0.24
19→28	1.57±0.11	1.61±0.11	1.61±0.12	1.70±0.13
28→35	1.53±0.12	1.56±0.12	1.56±0.15	1.59±0.17

HWHM which are similar to this measurement have previously been observed in the corresponding distributions extracted from the ${}^6\text{Li}(\pi^-, \text{nn}){}^4\text{He}$ and ${}^7\text{Li}(\pi^-, \text{nn}){}^5\text{He}$ data.⁴

The ${}^7\text{Li}(\pi^+, \text{pp}){}^5\text{He}$ data is similar to the ${}^6\text{Li}(\pi^+, \text{pp}){}^4\text{He}$ data discussed in Sec. V in that it can be described using T matrices which depend upon only two variables, P_R and θ'_1 . There appears to be no noticeable dependence of the T matrix upon the recoil momentum direction, (θ_R, ϕ_R) , over the phase space acceptance of our detector system.

Data were collected at two sets of angles which correspond to the center-of-mass angles $\theta'_1 = 68^\circ$ and 89° , respectively. The extracted values of the a_2 parameter for different transitions and angle sets are given in Table II. As discussed previously, the functional form given by Eq. (2) cannot completely describe the ground state transition or the transitions to the 16 to 19 MeV excitation region. For both regions the yield at recoil momentum above 150 MeV/c has a different θ'_1 dependence than the yield at smaller recoil momentum. This variation is reflected in the change in the value of a_2 as the upper cutoff in the recoil momentum distribution is increased from 150 to 300 MeV/c (Table II). The a_2 parameter calculated for the ground state increases from 1.13 up to 1.44. The a_2 parameter for the first excited state is consistent with the value 1.09. The numbers presented in Table II should be compared with the value 1.09, the a_2 parameter of the elementary $\pi^+ + d \rightarrow p + p$ reaction.⁹ The data for the sum of the ground state and 4 MeV state transitions, $-3 < E_x < 10$ MeV, averages the properties of the two different states and gives a value of a_2 consistent with 1.09 for all values of the cutoff recoil momentum (Table II, line 3). Thus with a high resolution measurement we are able to show that these two states require different values for the a_2 parameter thereby showing a deviation from the quasideuteron model that did not appear in earlier measurements.

The higher excited states show a different angular distribution, giving an a_2 parameter of about 1.6. Using the $\theta'_1 = 68^\circ$ data alone, which extend over an angular range of θ'_1 from 64° to 72° , gives $a_2 = -0.1 \pm 0.6$ indicating that the angular distribution is approximately flat over that range of angles. This result suggests that the functional form for the T matrices of the highly excited state transitions has an incorrect θ'_1 dependence and no serious attempt should be made to extrapolate into an unmeasured region of θ'_1 .

XI. THE ${}^7\text{Li}(\pi^+, \text{pp}){}^5\text{He}$ CROSS SECTIONS

Using the same procedure described in Sec. VI for the ${}^6\text{Li}(\pi^+, \text{pp}){}^4\text{He}$ reaction, the T matrix was normalized and triple-differential cross sections at $\theta_1 = 80.5^\circ$, $\theta_2 = 80.5^\circ$, $\phi_1 = 270^\circ$, $\phi_2 = 90^\circ$ were calculated and are shown in Fig. 17. The data for the ground state ($-3 < E_x < 1$ MeV) and 4 MeV state region ($1 < E_x < 10$ MeV) are well reproduced by the Monte Carlo simulation as is shown in Fig. 17. The Monte Carlo code is not as successful simulating the 28 to 35 MeV excitation region.

Using the functional form adopted here for the dependence of the T matrix upon P_R , θ_R , and ϕ_R (here isotropy is assumed in θ_R and ϕ_R), the triple-differential cross sections can be integrated over dE_1 and $d\Omega_2$ to get single-differential cross sections. These are given in Table III for cutoff recoil momentum of 200 and 300 MeV/c. The errors are statistical. A few percent of the cross section in the 16 to 19 MeV excitation region is likely to come from impurities (Sec. X). Only about 20% of the ground state single-differential cross section and 8% of the excited state single-differential cross section is contained within the phase space acceptance of the detectors.

The ${}^7\text{Li}(\pi^+, \text{pp}){}^5\text{He}$ and ${}^6\text{Li}(\pi^+, \text{pp}){}^4\text{He}$ single-

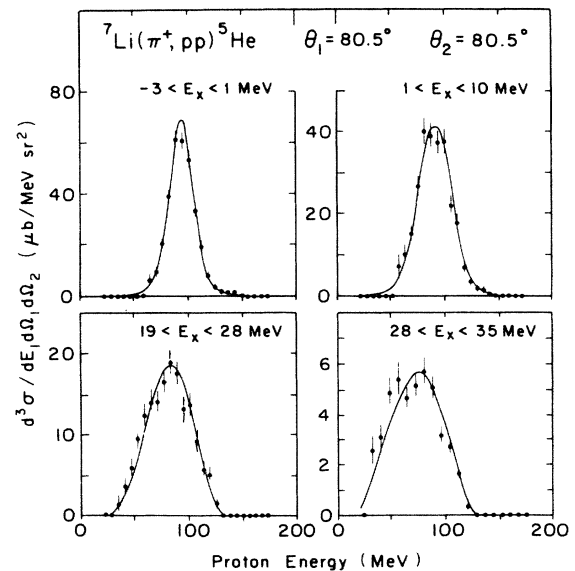


FIG. 17. The ${}^7\text{Li}(\pi^+, \text{pp}){}^5\text{He}$ triple-differential cross sections at $\theta_1 = 80.5^\circ$, $\phi_1 = 270^\circ$, $\theta_2 = 80.5^\circ$, $\phi_2 = 90^\circ$, for the excitation energy regions shown.

TABLE III. $d\sigma/d\Omega_1$ ($\mu\text{b}/\text{sr}$) for ${}^7\text{Li}(\pi^+, \text{pp}){}^5\text{He}$ (at $T=59.4$ MeV). Values show statistical errors and are based upon an extrapolation of a 20% (or 8%) measurement of the total yield.

Excitation energy (MeV)	Upper cutoff in recoil momentum (MeV/c)			
	$\theta_1=60^\circ$	200	$\theta_1=80.5^\circ$	300
$-3 \rightarrow 1$	407 ± 13		239 ± 5	583 ± 31
$1 \rightarrow 10$	463 ± 14		311 ± 7	576 ± 21
$16 \rightarrow 19$	248 ± 11		122 ± 4	360 ± 24
$19 \rightarrow 28$	811 ± 24		366 ± 8	1330 ± 51
$28 \rightarrow 35$	333 ± 12		192 ± 5	600 ± 20
				297 ± 8
				399 ± 11
				184 ± 7
				529 ± 12
				371 ± 9

differential cross sections at 60 deg have been compared with each other. The sum of the cross sections to the $\frac{3}{2}^-$ g.s. and $\frac{1}{2}^-$ first excited state in ${}^5\text{He}$ are 1.44 ± 0.6 times the cross section to the ${}^4\text{He}$ ground state. In the quasideuteron model, where the pion is absorbed on a (pn) pair in a spin triplet 3S_1 state, the cross sections should be in the ratio of 1.5 to 1. The agreement here with this model is excellent.

XII. SUMMARY

The ${}^6,7\text{Li}(\pi^+, \text{pp}){}^4,5\text{He}$ reactions were analyzed by fitting a T matrix to reproduce the data for each transition. From this analysis comes the first measured triple-differential cross sections for these reactions. These triple-differential cross sections are one-dimensional projections of our data out of a three-body final state in which there are five independent kinematic variables. A choice of functional form of the T matrices which depends upon only two kinematic variables could reproduce all of our data over the full phase space acceptance of our detectors.

The ${}^6\text{Li}(\pi^+, \text{pp}){}^4\text{He}$ ground state transition can be described in a model where the ${}^4\text{He}$ residual nucleus is a spectator; the measured properties of this transition appear to be identical to the elementary $\pi^+ + d \rightarrow p + p$ reaction. The T matrix for this transition has a dependence upon the recoil momentum, P_R , of the ${}^4\text{He}$ nucleus which is characteristic of an $L=0$ distribution, the momentum space wave function describing the relative motion of the ${}^4\text{He}$ and "deuteron" cluster in ${}^6\text{Li}$. This implies that the residual nucleus is left almost undisturbed by the reaction. The ${}^6\text{Li}(\pi^+, \text{pp}){}^4\text{He}$ ground state transition has nearly the same cross section as the elementary $\pi^+ + d \rightarrow p + p$ cross section. The magnitude, the dependence upon pion energy, and the dependence upon the directional angles of the outgoing protons is also nearly the same for both reactions. The similarity in the energy and angle dependence was inferred by comparing our data at $T_\pi=60$ MeV, $\theta_p=60^\circ$ with data at other energies and angles. The T -matrix analysis makes possible a simple method of comparing our data with the data at other energies and angles, including a comparison with (π^+, p) inclusive data.

The position of the Li isotopes, as transition nuclei for the (π^+, pp) reaction between the deuteron and heavier systems, is evident from our results. The T matrices for all transitions in lithium appeared to be simpler than for

pion absorption transitions in heavier nuclei,¹² i.e., ${}^{16}\text{O}(\pi^+, \text{pp}){}^{14}\text{N}$. They were similar to the predictions of a quasideuteron model in which the pion is absorbed on a 3S_1 (pn) cluster inside the lithium nucleus.

The most noticeable difference between the quasideuteron model and the data was in the ${}^7\text{Li}(\pi^+, \text{pp}){}^5\text{He}$ reaction to transitions removing a (pn) pair from the $(1s)^4$ alpha cluster in ${}^7\text{Li}$. The missing momentum, $\mathbf{P}_\pi - \mathbf{P}_1 - \mathbf{P}_2$, measured for these transitions has a broader distribution than would be predicted by the quasideuteron model, also, these transitions have a different proton-angular distribution than the elementary $\pi^+ + d \rightarrow p + p$ reaction (Sec. X). The ${}^7\text{Li}(\pi^+, \text{pp}){}^5\text{He}$ ground state transition also has a different proton angular distribution than the elementary $\pi^+ + d \rightarrow p + p$ reaction when the ${}^5\text{He}$ recoil momentum is greater than 150 MeV/c. For recoil momentum less than 150 MeV/c the two reactions have identical proton-angular distributions within experimental error. In general, the agreement of the data with the quasideuteron model is good.

Because the quasideuteron model works well, especially for the ${}^6\text{Li}(\pi^+, \text{pp}){}^4\text{He}$ transitions, we have used it to extrapolate our measured cross sections over the full three-body phase space and obtain integrated cross sections. The total ${}^6\text{Li}(\pi^+, \text{pp}){}^4\text{He}$ cross section at $T=60$ MeV is about 60 percent of the total pion absorption cross section on ${}^6\text{Li}$ at this energy. At first glance it appears presumptuous to extrapolate the ${}^6\text{Li}(\pi^+, \text{pp})$ measurements based upon a fraction of a percent measurement of the total yield. However it must be emphasized that the quasideuteron model succeeds in describing many detailed features of the ${}^6\text{Li}(\pi^+, \text{pp})$ reaction without having a single noteworthy failure.

It is reasonable to conclude with some confidence that the quasideuteron model is the correct description of our ${}^6\text{Li}(\pi^+, \text{pp})$ data. If this is true, there are only two types of situations which can result in the extrapolation being in error. The first type would be that some mechanism is suppressing the quasideuteron yield over a phase space region not covered by our detectors without affecting it over the measured phase space region. No such mechanism, to our knowledge, has ever been seriously contemplated and it is difficult to imagine this possibility. Such a suppression over a selected phase space is more difficult for a three-body final state than for a two-body final state. A two-body final state usually has a correlation between scattering angle, impact parameter, and momentum transfer, but the (π^+, pp) reactions should have no similar

correlations. We know that there is no noticeable suppression taking place over the measured phase space of our experiment nor over the measured phase space region of other experiments²¹ because the magnitude of the ${}^6\text{Li}(\pi^+,pp){}^4\text{He}$ g.s. transition is exactly what it is predicted to be according to the quasideuteron model. Its cross section at all measured angles and energies over the range from $T=50$ to 275 MeV is found to be slightly smaller than or equal to the elementary ${}^2\text{H}(\pi^+pp)$ cross section, as expected.

The second type of situation which can cause an error in the extrapolation is that other reaction mechanisms are supplying a significant yield in the unmeasured phase space without contributing significantly to the yield sampled by our detectors. This is a definite possibility. However, our extrapolation is already accounting for about 60 percent of the total pion absorption cross section at 59.4 MeV, and it is extremely unlikely that other (π^+,pp) mechanisms are accounting for a major fraction of the remaining 40 percent.

A recent experiment²⁷ has detected particles in coincidence following stopped π^- on ${}^6\text{Li}$. Among particle pairs consisting of all combinations of n, p, d, and t with relative angles between 150 and 180 deg in this experiment, 72.5% went into the (π^-,nn) channel. It is also known²⁸ that 83% of the π^- absorption at rest on ${}^3\text{He}$ (excluding pion charge exchange) goes into nn, np, and nd channels. Using this percentage as the fraction of pion absorption producing particle pairs in ${}^6\text{Li}$ and multiplying by 72.5% results in an estimation that 60% of the π^- absorption at rest goes into the (π^-,nn) channel. The (π^-,nn) channel is equivalent to the (π^+,pp) channel by

charge symmetry. This simple exercise shows that the extrapolation of our ${}^6\text{Li}^+(\pi^+,pp)$ data using the quasideuteron model is consistent with other existing low energy pion absorption data on ${}^6\text{Li}$.

Using the quasideuteron model, we have also extrapolated our cross section to pion energies of $T=160$ and 220 MeV to compare with the inclusive ${}^6\text{Li}(\pi^+,p)$ data.⁶ This extrapolation agrees reasonably well with the inclusive (π^+,p) data except for a 50% overestimation of the (π^+,p) cross section at 160 MeV. Even with an overestimation of the cross section, the quasideuteron model predicts that only 30% of the π^+ absorption cross section goes into the quasideuteron channel at 160 MeV. This happens because the pion total absorption cross section on ${}^6\text{Li}$ increases faster with pion energy than in the deuteron case.^{22,23}

All of the existing data, taken collectively, gives evidence that the fraction of pion absorption cross section attributable to the quasideuteron mechanism is decreasing significantly as the pion energy increases from 0 to 160 MeV. It appears to be about 60% at low energy, decreasing to less than 30% at 160 MeV. It will be interesting to see how well comprehensive models of pion absorption in nuclei can predict these systematics.

ACKNOWLEDGMENTS

We thank the staff at LAMPF for their cooperation and willingness to help meet the needs of this experiment. Paul Laughner, Joseph Sadecky, and Gary Wilkin are gratefully acknowledged for their efforts in the construction of much of the equipment.

*Permanent address: Physics Department, University of New Mexico, Albuquerque, NM 87131.

†Permanent address: Nuclear Physics Laboratory, University of Illinois, Champaign, IL 61820.

‡Permanent address: Brookhaven National Laboratory, Upton, NY 11973.

§Permanent address: Physics Department, Wheaton College, Wheaton, IL 60187.

**Permanent address: Physics Department, University of Pittsburgh, Pittsburgh, PA 15260.

††Present address: Lawrence Berkeley Laboratory, Berkeley, CA 94720.

¹J. Favier, T. Bressani, G. Charpak, L. Massonnet, W. E. Meyerhof, and C. Zupancic, Nucl. Phys. **A169**, 540 (1971).

²E. D. Arthur, W. C. Lam, J. Amato, D. Axen, R. L. Burman, P. Fessenden, R. Macek, J. Oostens, W. Shlaer, S. Sobotka, M. Salomon, and W. Swenson, Phys. Rev. C **11**, 332 (1975).

³R. L. Burman and M. E. Nordberg, Phys. Rev. Lett. **165**, 1096 (1968).

⁴B. Bassalleck, E. L. Haase, W. D. Klotz, F. Takeutchi, H. Ulrich, M. Furic, and Y. Sakamoto, Phys. Rev. C **19**, 1893 (1979).

⁵H. P. Isaak *et al.*, Helv. Phys. Acta **55**, 477 (1982).

⁶R. D. McKeown, S. J. Sanders, J. P. Schiffer, H. E. Jackson, M. Paul, J. R. Specht, E. J. Stephenson, R. P. Redwine, and R. E. Segel, Phys. Rev. C **24**, 211 (1981).

⁷R. H. Pehl, IEEE Trans. Nucl. Sci. NS-29, No. 3, 1101 (1982).

⁸J. F. Amann, P. D. Barnes, S. A. Dytman, J. A. Penkrot, A. C. Thompson, and R. H. Pehl, Nucl. Instrum. Methods **126**, 193 (1975).

⁹B. G. Ritchie, G. S. Blanpied, R. S. Moore, B. M. Preedom, K. Gotow, R. C. Minehart, J. Boswell, G. Das, H. J. Ziock, N. S. Chant, P. G. Roos, W. J. Burger, S. Gilad, and R. P. Redwine, Phys. Rev. C **27**, 1685 (1983).

¹⁰E. L. Haase, R. Hagelberg, and W. N. Wang, Nucl. Phys. **A188**, 89 (1972).

¹¹A. Van Der Woude and R. J. De Meijer, Nucl. Phys. **A258**, 199 (1976).

¹²W. R. Wharton, P. D. Barnes, B. Bassalleck, R. A. Eisenstein, G. Franklin, R. Grace, C. Maher, P. Pile, R. Rieder, J. Szymanski, J. R. Comfort, F. Taketutchi, J. F. Amann, S. A. Dytman, and K. G. R. Doss, Phys. Rev. C **31**, 526 (1985).

¹³D. Ashery, Proceedings of the Symposium on Delta-Nucleus Dynamics, 1983, edited by T. S. H. Lee, D. F. Geesaman, and J. P. Schiffer, Argonne National Laboratory Report Conf.-830588, 1983.

¹⁴N. F. Golovanova and N. S. Zelenskaya, Yad. Fiz. **8**, 274 (1968) [Sov. J. Nucl. Phys. **8**, 158 (1969)].

¹⁵I. Navo, E. Piasetzky, D. Ashery, A. Altman, G. Azuelos, F. W. Schlegel, and H. K. Walter, Phys. Lett. **95B**, 365 (1980).

¹⁶A. Altman, D. Ashery, E. Piasetzky, J. Lichtenstadt, A. I. Yavin, W. Bertl, L. Felawka, H. K. Walter, R. J. Powers, R. G. Winter, and J. V. D. Pluym, Phys. Lett. **144B**, 337 (1984).

¹⁷B. Karooglu, T. Karapiperis, and E. J. Moniz, Phys. Rev. C

- 22, 1984 (1806).
- ¹⁸J. P. Genin, J. Julien, M. Rambaut, C. Samour, A. Palmeri, and D. Vinciguerra, *Phys. Lett.* **52B**, 46 (1974).
- ¹⁹D. Albrecht, M. Csatlos, J. Ero, Z. Fodor, I. HERNYES, Hong-sung Mu, B. A. Khomenko, N. N. Khovanskij, P. Koncz, Z. V. Krumstein, Yu P. Merekov, V. I. Petrukhin, Z. Seres, and L. Vegh, *Nucl. Phys.* **A338**, 477 (1980).
- ²⁰D. R. Lehman, *Phys. Rev. C* **25**, 3146 (1982).
- ²¹T. Bressani, G. Charpak, J. Favier, L. Massonnet, W. E. Meyerhof, and C. Zupancic, *Nucl. Phys.* **B9**, 427 (1969).
- ²²I. Navon, D. Ashery, J. Alster, G. Azuelos, B. M. Barnett, W. Byles, R. R. Johnson, D. R. Gill, and T. G. Masterdon, *Phys. Rev. C* **28**, 2548 (1983).
- ²³D. Ashery, I. Navon, G. Azuelos, H. K. Walter, H. J. Peiffer, and F. W. Schlepütz, *Phys. Rev. C* **23**, 2173 (1981).
- ²⁴W. R. Wharton, *Pion Production and Absorption in Nuclei—1981 (Indiana University Cyclotron Facility)*, Proceedings of the Pion Production and Absorption in Nuclei, AIP Conf. Proc. No. 79, edited by R. D. Bent (AIP, New York, 1982), p. 371.
- ²⁵M. P. Baker, J. M. Cameron, N. S. Chant, and N. F. Mangelson, *Nucl. Phys.* **A184**, 97 (1972).
- ²⁶J. Ero, Z. Fodor, P. Koncz, Z. Seres, M. Csatlos, B. A. Khomenko, N. N. Khovanskij, Z. V. Krumstein, Yu P. Merekov, and V. I. Petrukhin, *Nucl. Phys.* **A372**, 317 (1981).
- ²⁷M. Dorr, W. Fetscher, D. Gotta, J. Reich, H. Ullrich, G. Backenstoss, W. Kowald, and J. J. Weyer, *Nucl. Phys. A* (to be published).
- ²⁸P. Truöl, H. W. Bear, J. A. Bistirlich, K. M. Crowe, N. deBotton, and J. A. Helland, *Phys. Rev. Lett.* **32**, 1268 (1974).